Many-Body Invariants for Chern and Chiral Hinge Insulators

Byungmin Kang, Wonjun Lee, and Gil Young Cho

Phys. Rev. Lett. **126**, 016402 — Published 6 January 2021

DOI: 10.1103/PhysRevLett.126.016402

Many-Body Invariants for Chern and Chiral Hinge Insulators

Byungmin Kang,[1,*] Wonjun Lee,[2,†] and Gil Young Cho[2,3,4,‡]

[1] *School of Physics, Korea Institute for Advanced Study, Seoul 02455, Korea*
[2] *Department of Physics, Pohang University of Science and Technology (POSTECH), Pohang 37673, Republic of Korea*
[3] *Asia Pacific Center for Theoretical Physics, Pohang, Republic of Korea*
[4] *Center for Artificial Low Dimensional Electronic Systems, Institute for Basic Science (IBS), Pohang 37673, Republic of Korea*

(Dated: December 4, 2020)

We construct new many-body invariants for 2d Chern and 3d chiral hinge insulators characterizing quantized pumping of bulk dipole and quadrupole moments. The many-body invariants are written entirely in terms of many-body ground state wavefunctions on a torus geometry with twisted boundary conditions and a set of unitary operators. We present a number of supporting evidences for the invariants via topological field theory interpretation, adiabatic pumping argument, and direct mapping to free-fermion band indices. Therefore, the invariants explicitly encircle several different pillars of theoretical descriptions of topological phases. Furthermore, our many-body invariants are written in forms which can directly be employed in various numerics including the exact diagonalization and the density-matrix renormalization group simulations. We finally confirm our invariants by numerical computations including infinite density matrix renormalization group on quasi-one-dimensional systems.

1. Introduction: The discovery of topological band insulators initiated a serious revisit to the band theory of insulators, which has fruited in the last fifteen years.[1,2] So far, the classification of the band topology has made a remarkable success and found numerous topological insulators.[3–6] Moreover, insightful band indices and underlying structures[1,2,7] have been revealed. One particular progress, which attracted a huge attention recently, is the so-called higher-order topological insulators,[7–10] whose topology manifests as the symmetry-protected corner or hinge states instead of more familiar surface states. However, the understanding of higher-order topological insulators has been limited mostly to non-interacting band insulators, except for a few cases.[11,12] This is in stark contrast to their ancestors, e.g., insulators with bulk polarization[13] and Chern insulators,[14] where one can define and detect the topology even without referring to the band structure. For instance, the Resta's formula[13] measures the polarization in a non-perturbative fashion for any insulators.

In this Letter, we propose many-body invariants for prototypical chiral topological phases, i.e., 2d Chern insulator[14] and 3d chiral hinge insulator.[7–9] Two insulators are characterized by quantized chiral pumping of bulk quantum numbers under the adiabatic change of the background $U(1)$ gauge field. We show that how our many-body invariants directly measure the bulk topology of such chiral pumpings within the many-body wavefunctions by generalizing Resta's pioneering work.[13] We combine different theoretical approaches to support the validity of our invariants: many-body adiabatic pumping argument, topological field theory interpretation, and reduction to free-fermion band indices. We finally confirm our invariants via numerical calculations.

The many-body invariants[11–13,15] can be applied to correlated states of matter[16] and to systems without translational symmetries. Even for clean and non-interacting systems, the invariants provide a complementary diagnosis to the free-electron momentum-space band indices.[17–20] Not only practically but also fundamentally, the construction of many-body invariants is important on its own, as it can provide a classification of the quantum phases of matter in the most general setups.

Many-body invariants for Chern insulators has been intensively studied since the seminal paper by Niu, Thouless, and Wu.[21] Using the "effective" Brillouin zone where the twisted boundary conditions replaces the role of Bloch momenta, many-body Chern number can be expressed as an integral of many-body Berry curvature over the effective Brillouin zone.[21,22] While the integral guarantees the quantization of the many-body Chern number, Hastings and Michalakis[23] showed that the many-body Berry curvature itself is quantized up to a 'almost-exponentially' decaying error term in system size when the bulk gap is non-zero. This leads to the one-plaquette formula for the many-body Chern number.[24] Finally, a many-body formula, which tracks the winding of the y-direction many-body polarization as a function of x-direction flux Φ_x, appeared in Ref. 25.

In this Letter, we consider the following function defined in terms of many-body ground state wavefunctions:

$$\mathcal{Z}[\Phi_a] = \frac{\langle \mathrm{GS}[\Phi_a]|\hat{U}_{\mathrm{top}}|\mathrm{GS}[\Phi_a]\rangle}{\langle \mathrm{GS}[0]|\hat{U}_{\mathrm{top}}|\mathrm{GS}[0]\rangle}, \tag{1}$$

where we use *two and only two* many-body ground states $|\mathrm{GS}[\Phi_a]\rangle$ on a torus geometry, whose boundary condition along the a-direction of the torus is twisted by a flux Φ_a, whereas other directions are chosen to be periodic without twisting. We choose $\hat{U}_{\mathrm{top}}$ depending on the bulk topology of interest. We will show below that the many-body invariant is encoded in the $U(1)$ phase factor of $\mathcal{Z}[\Phi_a]$.

For the systems of our interest, it is sufficient to consider only two unitaries: Resta's polarization operator along the j-direction,[13]

$$\hat{U}_{1,j} = \exp\Big(\frac{2\pi i}{L_j}\sum_{\boldsymbol{r}} x_j \hat{n}(\boldsymbol{r})\Big), \tag{2}$$

and the quadrupole operator along the xy-plane from our previous work[11,12]

$$\hat{U}_2 = \exp\Big(\frac{2\pi i}{L_x L_y}\sum_{\boldsymbol{r}} xy\hat{n}(\boldsymbol{r})\Big). \tag{3}$$

We assume that two unitary operators can measure the bulk dipole and quadrupole moments of many-body insulators under appropriate conditions.[26]

2. Chern Insulator: We first construct the many-body invariant for the many-body Chern number from many-body wavefunctions $|\mathrm{GS}[\Phi_x]\rangle$ defined on a torus geometry, where the flux Φ_x along the x-direction is chosen to be small. We encode the flux via coupling the system to the uniform gauge field $A_x = \frac{\Phi_x}{L_x}$. Finally, we obtain the *many-body* Chern number C by

$$\mathcal{Z}_c[\Phi_x] = \frac{\langle \mathrm{GS}[\Phi_x]|\hat{U}_{1,y}|\mathrm{GS}[\Phi_x]\rangle}{\langle \mathrm{GS}[0]|\hat{U}_{1,y}|\mathrm{GS}[0]\rangle} = |\mathcal{Z}|\exp\big(iC\Phi_x\big). \tag{4}$$

While our formula Eq. (4) only approximates the quantized many-body Chern number C for a finite system with finite flux Φ_x, it recovers the quantized C in the thermodynamic limit, i.e., first take $\Phi_x \to 0^+$ for each system size and then take the system size to infinity, when the bulk gap remains finite. For the details on the finite size effects and comparison between Eq. (4) and the previous ones,[21–25] please refer to the Supplemental Material (SM).[26]

To justify of our formula, we first prove that C in Eq. (4) reduces to the band Chern number for non-interacting band insulators. While sketching the key steps below, we defer a more complete derivation to SM.[26] In a non-interacting fermion system, one first constructs single-particle eigenstates $|\boldsymbol{k}\rangle \otimes |u(\boldsymbol{k})\rangle$, where $|\boldsymbol{k}\rangle$ is the plane wave labeled by the (Bloch) momentum and $|u(\boldsymbol{k})\rangle$ is the corresponding Bloch state. The ground state is given by the Slater determinant of the occupied single-particle states. Note that the flux Φ_x merely modifies the allowed set of momentum $\boldsymbol{k}$. For a single filled band insulator, Eq. (4) becomes

$$\mathcal{Z}_c = \frac{\prod_{k_x,k_y}\big\langle u\big(k_x + \frac{\Phi_x}{L_x}, k_y\big)\big|u\big(k_x + \frac{\Phi_x}{L_x}, k_y + \frac{2\pi}{L_y}\big)\big\rangle}{\prod_{k_x,k_y}\big\langle u(k_x,k_y)\big|u\big(k_x, k_y+\frac{2\pi}{L_y}\big)\big\rangle},$$

where the products in the denominator and the numerator are over the same set of momenta, i.e., $k_a = \frac{2\pi}{L_a}n_a$ with $n_a \in \{1, 2, \cdots L_a\}$ and L_a being the linear system size in the a-direction. For L_a large, we can approximate

$$\begin{aligned}\mathcal{Z}_c &\approx \frac{\prod_{k_x}\exp\Big[i\int dk_y \mathcal{A}_y(k_x + \frac{\Phi_x}{L_x}, k_y)\Big]}{\prod_{k_x}\exp\Big[i\int dk_y\mathcal{A}_y(k_x,k_y)\Big]} \\ &= \frac{\prod_{k_x}\exp\Big[2\pi i\mathcal{P}_y(k_x + \frac{\Phi_x}{L_x})\Big]}{\prod_{k_x}\exp\Big[2\pi i \mathcal{P}_y(k_x)\Big]},\end{aligned}$$

where $\mathcal{P}_y(k_x)$ is the y-directional polarization for a given momentum k_x. Finally, Eq. (4) reduces to:

$$\begin{aligned}\mathcal{Z}_c &= \prod_{k_x}\exp\Big[2\pi i\Big(\mathcal{P}_y\Big(k_x + \frac{\Phi_x}{L_x}\Big) - \mathcal{P}_y(k_x)\Big)\Big] \\ &\approx \exp\Big[i\Phi_x\int_0^{2\pi} dk_x \frac{d\mathcal{P}_y(k_x)}{dk_x}\Big] = \exp(i\Phi_x C),\end{aligned} \tag{5}$$

where we have identified the change in the polarization $\mathcal{P}_y$ in k_x as the Chern number.[27] The multiband case is presented in the SM.[26]

We now employ the many-body adiabatic pumping to show that Eq. (4) must be related to the Hall conductivity σ_{xy}. We first note that the Resta operator $\hat{U}_{1,y}$ measures the many-body polarization.[26] Using the Resta operator,

$$\mathcal{Z}_c \propto \exp\Big[2\pi i\left(\mathrm{P}_y(\Phi_x) - \mathrm{P}_y(0)\right)\Big],$$

where $\mathrm{P}_y(\Phi_x)$ is the many-body polarization along the y-direction for the ground state under the flux Φ_x. Note that for band insulators, $\mathrm{P}_y(\Phi_x) = \sum_{k_x}\mathcal{P}_y\big(k_x + \frac{\Phi_x}{L_x}\big)$. When Φ_x is small,

$$\mathcal{Z}_c \approx \exp\Big[2\pi i\Phi_x\frac{d\mathrm{P}_y}{d\Phi_x}\Big] = \exp\Big[2\pi i\Phi_x\sigma_{xy}\Big] = \exp\Big(iC\Phi_x\Big),$$

where we used the fact that the change in the polarization P_y in the ground state can be induced by the adiabatic change in the flux Φ_x, i.e., $\frac{d\mathrm{P}_y}{d\Phi_x} = \frac{d\mathrm{P}_y/dt}{d\Phi_x/dt} = \frac{J_y}{E_x} = \sigma_{xy}$, and the last equality follows from $\sigma_{xy} = \frac{C}{2\pi}$. Since we did not assume that the ground state is a band insulator, we expect that Eq. (4) can be applied beyond band insulators.

The final proof of Eq. (4) is via the topological field theory. To this end, we show that the many-body invariant picks up the level C of the Chern-Simons action,

$$S_{eff} = \frac{C}{4\pi}\int d\tau d^2x\ \epsilon^{\mu\nu\lambda}A_\mu\partial_\nu A_\lambda, \tag{6}$$

which is the effective field theory of the Chern insulator with the Chern number C. We emphasize again that we do not make any assumption on the ground state hence Eq. (4) applies to any correlated insulators. We get[26]

$$\langle \mathrm{GS}[\Phi_x]|\hat{U}_{1,y}|\mathrm{GS}[\Phi_x]\rangle \propto \exp\Big(iS_{eff}[A_\mu]\Big) = \exp\left(i\Phi_x C\right),$$

where A_μ is fixed by the twisted boundary condition Φ_x and the insertion of the unitary $\hat{U}_{1,y}$, i.e, $(A_0; A_x, A_y) = \left(\delta(\tau)\frac{2\pi}{L_y}y; \frac{\Phi_x}{L_x}, 0\right)$. By inserting this gauge configuration into Eq. (6), we indeed find that the level C appears in the RHS of the above equation. We note that the same approach for multipole insulators has been employed before.[11]

3. Chiral Hinge Insulator: We now present the many-body invariant for C_4T-symmetric chiral hinge insulators:[7–9]

$$\mathcal{Z}_h[\Phi_z] = \frac{\langle \mathrm{GS}[\Phi_z]|\hat{U}_2|\mathrm{GS}[\Phi_z]\rangle}{\langle \mathrm{GS}[0]|\hat{U}_2|\mathrm{GS}[0]\rangle} = |\mathcal{Z}|\exp(i\Phi_z C_W), \quad (7)$$

where $|\mathrm{GS}[\Phi_z]\rangle$ is the ground state with the boundary condition along the z-axis being twisted by an infinitesimal Φ_z. We explicitly see below that C_W is the integer labeling the quantized pumping of the quadrupole moment under the adiabatic insertion of the flux Φ_z. Similar to Eq. (4), Eq. (7) contains finite size effects which is expected to vanish in the thermodynamic limit when the bulk gap is nonzero. For a band insulator, C_W equals the Wannier-sector Chern number.[28]

To justify our many-body invariant, we first reduce Eq. (7) to a band index, which computes the quantized pumping of the quadrupole moment along k_z. As before, many-body ground state is given by the Slater determinant of occupied single-particle eigenstates. The single-particle states are given by the Bloch functions $|u_n(\boldsymbol{k}_\perp, k_z)\rangle$ and the plane waves $|\boldsymbol{k}_\perp, k_z\rangle$, i.e., $|\psi_n(\boldsymbol{k}_\perp, k_z)\rangle = |\boldsymbol{k}_\perp, k_z\rangle \otimes |u_n(\boldsymbol{k}_\perp, k_z)\rangle$ with n labeling the filled bands and $\boldsymbol{k}_\perp$ being the momentum in the xy-plane. The many-body invariant Eq. (7) is then reduces to

$$\mathcal{Z}_h = \frac{\prod_{k_z}\prod_{\boldsymbol{k}_\perp,\boldsymbol{k}'_\perp} \mathcal{F}(\boldsymbol{k}'_\perp, \boldsymbol{k}_\perp, k_z + \frac{\Phi_z}{L_z})}{\prod_{k_z}\prod_{\boldsymbol{k}_\perp,\boldsymbol{k}'_\perp} \mathcal{F}(\boldsymbol{k}'_\perp, \boldsymbol{k}_\perp, k_z)}, \quad (8)$$

where the momentum k_z in the products is over the set $k_z \in \{\frac{2\pi}{L_z}n_z, n_z = 0, 1, \cdots L_z - 1\}$, and similarly for $\boldsymbol{k}$ and $\boldsymbol{k'}$. Here, $\mathcal{F}$ is defined in terms of the Bloch functions:

$$\begin{aligned}
&\mathcal{F}\Big(\boldsymbol{k}'_\perp, \boldsymbol{k}_\perp, k_z + \frac{\Phi_z}{L_z}\Big) \\
&= \det\left[\Big\langle \boldsymbol{k}'_\perp, k_z + \frac{\Phi_z}{L_z}\Big| e^{\frac{i2\pi xy}{L_x L_y}}\Big|\boldsymbol{k}_\perp, k_z + \frac{\Phi_z}{L_z}\Big\rangle \right. \\
&\qquad \left. \times \Big\langle u_n\Big(\boldsymbol{k}'_\perp, k_z + \frac{\Phi_z}{L_z}\Big)\Big| u_m\Big(\boldsymbol{k}_\perp, k_z + \frac{\Phi_z}{L_z}\Big)\Big\rangle\right],
\end{aligned}$$

where the matrix in the determinant by writing are denoted by its component. Using the fact that $\hat{U}_2$ measures the bulk quadrupole moment,[11,12] we identify

$$\prod_{\boldsymbol{k}_\perp,\boldsymbol{k}'_\perp} \mathcal{F}\Big(\boldsymbol{k}'_\perp, \boldsymbol{k}_\perp, k_z + \frac{\Phi_z}{L_z}\Big) = \exp\left[2\pi i \mathcal{Q}_{xy}\Big(k_z + \frac{\Phi_z}{L_z}\Big)\right],$$

where $\mathcal{Q}_{xy}(k_z)$ is the xy quadrupole moment for a given k_z. Finally, Eq. (8) for an infinitesimal Φ_z becomes

$$\begin{aligned}
\mathcal{Z}_h &= \prod_{k_z} \exp\left[2\pi i\Big(\mathcal{Q}_{xy}\Big(k_z + \frac{\Phi_z}{L_z}\Big) - \mathcal{Q}_{xy}(k_z)\Big)\right] \\
&\approx \exp\left[i\Phi_z \int_0^{2\pi} dk_z \frac{d\mathcal{Q}_{xy}(k_z)}{dk_z}\right] = \exp\Big[i\Phi_z C_W\Big],
\end{aligned}$$

i.e., Eq. (8) measures the chiral pumping of quadrupole moment $\mathcal{Q}_{xy}(k_z)$ along k_z, as advertised.

Remarkably, our formula Eq. (7) is consistent with the effective field theory of the chiral hinge insulator proposed in Ref. [29]:

$$S^h_{eff} = \frac{C_W}{4\pi}\int d\tau d^3x\ A_z\left(\partial_t\partial_y A_x + \partial_t\partial_x A_y - 2\partial_x\partial_y A_0\right).$$

We first note that[26]

$$\langle \mathrm{GS}|\hat{U}_2|\mathrm{GS}\rangle \propto \exp\Big(iS^h_{eff}[A_\mu]\Big),$$

where A_μ is fixed by the twisted boundary condition Φ_z and the insertion of the unitary $\hat{U}_2$, i.e, $(A_0; A_x, A_y, A_z) = (\delta(\tau)\frac{2\pi xy}{L_y L_x}; 0, 0, \frac{\Phi_z}{L_x})$. By inserting this gauge field configuration to the effective field theory, we find Eq. (7). Note that the effective topological field theory description is valid for interacting and/or disordered cases, implying that the same is true for Eq. (7).

Finally, we discuss the physics hidden behind Eq. (7). Our discussion below highlights the relation between our formula Eq. (7) and the Wannier-sector Chern number.[11,12] We first note that the ground state overlaps in Eq. (7) give the bulk quadrupole moments along the xy-direction of the ground states:

$$\mathcal{Z}_h \propto \exp\Big[2\pi i\left(\mathrm{Q}_{xy}(\Phi_z) - \mathrm{Q}_{xy}(0)\right)\Big],$$

where $\mathrm{Q}_{xy}(\Phi_z)$ is the xy-plane quadrupole moment of the ground state under the flux Φ_z. Assuming that Q_{xy} is a smooth function of Φ_z, we find:

$$\mathcal{Z}_h \propto e^{2\pi i\Phi_z \frac{d\mathrm{Q}_{xy}}{d\Phi_z}} = e^{2\pi i\Phi_z \frac{d\mathrm{Q}_{xy}/dt}{d\Phi_z/dt}} = e^{2\pi i\Phi_z \frac{J^{\mathrm{quad}}_{xy}}{E_z}}., \quad (9)$$

where we note that an adiabatic change of the flux Φ_z induces the electric field along the z-direction on the surface. The change in quadrupole moment is then given by the surface current J_{quad} perpendicular to the z-direction. By demanding that the last expression of Eq. (9) to be equivalent to Eq. (7), we find

$$\sigma^{\mathrm{quad}}_{xy} = \frac{J^{\mathrm{quad}}_{xy}}{E_z} = \frac{C_W}{2\pi}.$$

This process is precisely what one expects from the nested Wilson loop picture,[8] and hence provides an additional supporting evidence for our formula. We complete the comparison by performing another transformation on Eq. (9). Let us rewrite J^{quad}_{xy} as the variation of the quadrupolar surface orbital magnetization M_{xy}^{quad}, i.e, $J_{xy}^{\text{quad}} = \frac{dM_{xy}^{\text{quad}}}{dz}$. Similarly, we rewrite $E_z = \frac{d\mu^s}{dz}$, where μ^s is the surface chemical potential. Then, we find

$$\mathcal{Z}_h = e^{2\pi i \Phi_z \frac{J_{xy}^{\text{quad}}}{E_z}} \to e^{2\pi i \Phi_z \frac{dM_{xy}^{\text{quad}}}{d\mu^s}}.$$

By equating the last expression to the one in Eq. (9), we find

$$\frac{dM_{xy}^{\text{quad}}}{d\mu^s} = \frac{C_W}{2\pi}.$$

This is again consistent with the nested Wilson loop picture[8] and the orbital magnetization calculation.[30] Hence, starting from Eq. (7), we derive the following quadrupolar "Streda formula":

$$\frac{dQ_{xy}}{d\Phi_z} = \frac{J_{xy}^{\text{quad}}}{E_z} = \frac{dM_{xy}^{\text{quad}}}{d\mu^s} = \frac{C_W}{2\pi}, \tag{10}$$

which is consistent with the effective field theory description.[29]

4. Numerical demonstrations: In this section, we provide numerical confirmations of our many-body invariants Eqs. (4) and (7) for the Chern and chiral hinge insulators. We numerically compute the invariants for various insulators including band insulators, non-interacting insulators without translational symmetry, and correlated insulators. In all cases, our many-body invariants faithfully measure the bulk topological invariants.

We begin with two tight-binding models of Chern insulators[31] on a square lattice:

$$\hat{H}_{\text{Ch}}^{(1)} = \sum_{\boldsymbol{k}} c_{\boldsymbol{k}}^\dagger \big[(m - t\cos(k_x) - t\cos(k_y))\sigma_z + \Delta\sin(k_x)\sigma_x + \Delta\sin(k_y)\sigma_y\big] c_{\boldsymbol{k}} \tag{11}$$

and

$$\hat{H}_{\text{Ch}}^{(2)} = \sum_{\boldsymbol{k}} c_{\boldsymbol{k}}^\dagger \big[(m - t\cos(k_x) - t\cos(k_y))\sigma_z + \Delta_1(\cos(k_x) - \cos(k_y))\sigma_y + \Delta_2\sin(k_x)\sin(k_y)\sigma_x\big] c_{\boldsymbol{k}} \tag{12}$$

where $c_{\boldsymbol{k}}^\dagger = (c_{\boldsymbol{k},A}^\dagger, c_{\boldsymbol{k},B}^\dagger)$ with A and B labeling the orbitals. By tuning m while keeping t and Δ ($\{\Delta_1, \Delta_2\}$) fixed, the half-filled ground state of $\hat{H}_{\text{Ch}}^{(1)}$ ($\hat{H}_{\text{Ch}}^{(2)}$) realizes the quantum phase transitions between $C = \pm 1$ ($C = \pm 2$) Chen insulator to trivial insulator. In FIG. 1 (a) and (b), we confirm that our many-body invariant Eq. (4) reproduces the phase diagrams of $\hat{H}_{\text{Ch}}^{(1)}$ and $\hat{H}_{\text{Ch}}^{(2)}$.

For a further confirmation of Eq. (4), we consider a tight-binding model with onsite random disorder by adding position dependent mass terms $\sum_{\boldsymbol{r}} m_{\boldsymbol{r}} c_{\boldsymbol{r}}^\dagger \sigma_z c_{\boldsymbol{r}}$, where $c_{\boldsymbol{r}}^\dagger = (c_{\boldsymbol{r},A}^\dagger, c_{\boldsymbol{r},B}^\dagger)$ and $m_{\boldsymbol{r}} \in [0, W]$ with W controlling the disorder strength. In FIG. 1 (c), we see that

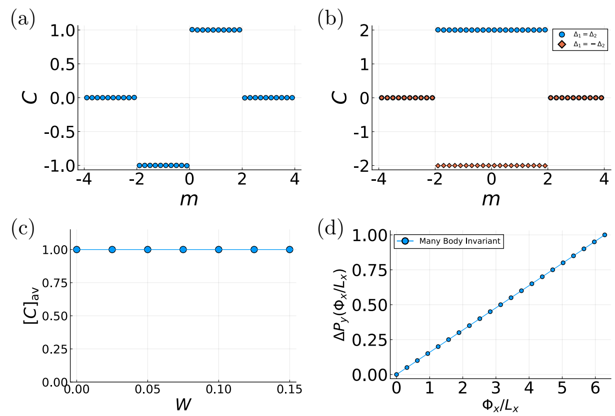

FIG. 1. The Chern numbers from Eq. (4) for (a) $\hat{H}_{\text{Ch}}^{(1)}$ with $(t, \Delta) = (1.0, 1.0)$ and (b) $\hat{H}_{\text{Ch}}^{(2)}$ with $(t, \Delta_1, \Delta_2) = (1.0, 1.0, \pm 1.0)$ as a function of m. (c) The disorder averaged Chern number as a function of disorder strength W. We fix $(t, m, \Delta) = (1.0, 1.0, 1.0)$ in Eq. (11) and add additional position dependent mass term according to $m_{\boldsymbol{r}} \in [0, W]$. $[C]_{\text{av}}$ is computed over 1000 disorder realizations. (d) Change in the y-polarization per unit x-length as a function of x-flux per unit x-length Φ_x/L_x for $\hat{H}_{\text{Ch}}^{(1)} + \hat{H}_U$. We use the parameters $(t, m, r; U) = (1.0, 1.0, 1.0; 1.0)$, $N_y = 4$, and the bond dimension $\chi = 100$ in the iDMRG simulations.

the disorder averaged Chern number $[C]_{\text{av}}$ computed using Eq. (4) stays quantized as a function of W. This shows the stability of our formula against adding weak disorder. Cases with strong disorder are discussed in the SM.[26]

Next, we consider an interacting model $\hat{H} = \hat{H}_{\text{Ch}}^{(1)} + \hat{H}_U$, where $\hat{H}_U = U \sum_{\boldsymbol{r}} c_{\boldsymbol{r},A}^\dagger c_{\boldsymbol{r},A} c_{\boldsymbol{r},B}^\dagger c_{\boldsymbol{r},B}$ is an onsite Hubbard interaction. We perform an infinite density-matrix renormalization group (iDMRG) simulation[32,33] on the infinite cylindrical geometry. We choose the x-axis as the infinite cylindrical axis direction and the y-direction as the finite circumference direction containing L_y sites. From the infinite matrix product states (iMPS) generalization of Eq. (4),[26] we can extract the Chern number using two iMPS ground states—one without any flux insertion and the other with an infinitesimal flux-per-unit-length inserted along the x-direction.

Our method bears some similarity with the usual method[34] for measuring the Chern number in the iDMRG simulations. In fact, both methods measure the identical observables if L_y is sufficiently large. However, when L_y is finite and small, as in the usual iDMRG simulations on quasi-1d systems, two methods measure the Chern number differently. The usual method[34] measures the polarization along the infinite x-direction *exactly*, but twisting the boundary condition *adiabatically* by threading the flux Φ_y from 0 to 2π along the finite y-direction. Since the allowed momentum along the y-direction is highly restricted due to the smallness of L_y, it is important to keep track of the winding of the x-polarization via full adiabatic changes of Φ_y. On the other hand, our method measures the polarization along the y-direction *approximately* using $\hat{U}_{1,y}$ operator, but only requires an *infinitesimal* gauge flux along the infinite x-direction. Since the momentum along the infinite direction is fully available, it is sufficient to consider the states with zero and an infinitesimal flux-per-unit-length. In the iDMRG simulation, we use the parameters where the ground state of $\hat{H}^{(1)}_{\rm Ch} + \hat{H}_U$ is adiabatically connected to the $U = 0$ ground state. In FIG. 1 (d), we see that the y-directional polarization-per-unit-length computed from our formalism shows perfect linear behavior as a function of the x-flux-per-unit-length Φ_x/L_x, thereby indicating that the many-body invariant for iMPS ground states sincerely computes the many-body Chern number. In the SM,[26] we showed that our many-body invariant captures a trivial Mott insulating regime where U is large.

Finally, we numerically confirm the many-body invariant Eq. (7) for C_4T-symmetric chiral hinge insulators. We consider the following tight-binding model:[9]

$$\hat{H}_{\rm Hinge} = \sum_{\boldsymbol{k}} c^\dagger_{\boldsymbol{k}} \big[(m - t \sum_{i=x,y,z} \cos(k_i))\tau_z\sigma_0 \tag{13}$$

$$+ \Delta_1 \sum_{i=x,y,z} \sin(k_i)\tau_x\sigma_i + \Delta_2(\cos(k_x) - \cos(k_y))\tau_y\sigma_0\big] c_{\boldsymbol{k}},$$

where $c_{\boldsymbol{k}} = (c_{\boldsymbol{k},A,\uparrow}, c_{\boldsymbol{k},A,\downarrow}, c_{\boldsymbol{k},B,\uparrow}, c_{\boldsymbol{k},B,\downarrow})^T$. In FIG. 2 (a), we use the many-body invariant Eq. (7) to compute C_W as a function of the mass parameter m with fixed (t, Δ_1, Δ_2). The many-body invariant Eq. (7) reproduces the phase diagram up to finite size effects.

For a final non-trivial test, we add an onsite Hubbard interaction $U \sum_{\boldsymbol{r},a=A,B} \hat{n}_{\boldsymbol{r},a,\uparrow}\hat{n}_{\boldsymbol{r},a,\downarrow}$ to Eq. (13). Interaction effects are captured via self-consistent Hartree-Fock method which variationally finds the energy minimizing single Slater determinant state. We turn on small U so that the ground state is adiabatically connected to the $U = 0$ ground state. The phase factor of the many-body invariant Eq. (7) are tracked under the full 2π flux insertion along the z-direction. In FIG. 2 (b), we see perfect linear behaviors with the slopes equal C_W as expected.

There exists chiral hinge insulators where the chiral modes originated from boundary Chern bands, not from the bulk quadrupole moments, i.e., $C_W = 0$ in Eq. (7). Detection of these insulators using Eq. (1) and the applicability of $\hat{U}_2$ in measuring boundary observables will be reported elsewhere.[35]

5. Conclusions: We have provided many-body invariants for 2d Chern and 3d chiral hinge insulators. Our many-body invariants have natural interpretations in terms of three different theoretical approaches: many-body adiabatic pumping, topological field theory, and reduction to free-fermion band indices. Our invariants provide not only a unified theoretical framework of understanding various chiral insulators, but also efficient ways of computing bulk topological numbers as the invariants require only two ground states and are easily implementable in various numerics. We have tested our formula for various non-interacting models with and without translation symmetries, and interacting models. In all cases, we see that our invariants faithfully detect the ground state topology.

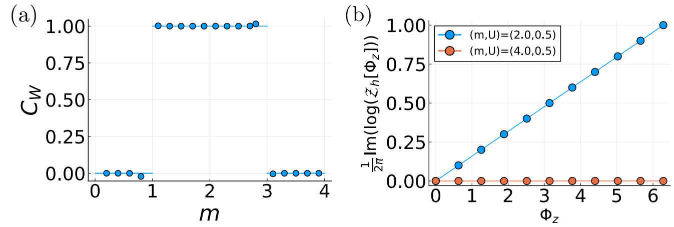

FIG. 2. (a) C_W from Eq. (7) for the half-filled ground state of Eq. (13) with $(t, \Delta_1, \Delta_2) = (1.0, 1.0, 1.0)$, system size $(L_x, L_y, L_z) = (20, 20, 40)$, and $\Phi_z = 0.01$. (b) Change in the phase factor of $\mathcal{Z}_h(\Phi_z)$ as a function of Φ_z. The ground states are constructed using the Hartree-Fock approximation. We fix $(t, \Delta_1, \Delta_2) = (1.0, 1.0, 1.0)$ and use the linear system size $L = 10$. We see perfect linear behaviors in both cases where the slopes capture the correct C_W.

ACKNOWLEDGMENTS

We thank Barry Bradlyn, Jong Yeon Lee, Masaki Oshikawa, and Aaron Szasz for helpful discussion. BK was supported by KIAS individual Grant PG069401 at Korea Institute for Advanced Study and the National Research Foundation of Korea (NRF) grant funded by the Korea government (MSIT) (No. 2020R1F1A1075569). WL and GYC are supported by the National Research Foundation of Korea (NRF) grant funded by the Korea government(MSIT) (No.2020R1C1C1006048 and No.2020R1A4A3079707) and by IBS-R014-D1. This work was supported by the Center for Advanced Computation at Korea Institute for Advanced Study.

* Electronic Address: bkang119@kias.re.kr
† Electronic Address: wonjun1998@postech.ac.kr
‡ Electronic Address: gilyoungcho@postech.ac.kr

1 M. Z. Hasan and C. L. Kane, "Colloquium: Topological insulators," Rev. Mod. Phys. **82**, 3045–3067 (2010).
2 Xiao-Liang Qi and Shou-Cheng Zhang, "Topological insulators and superconductors," Rev. Mod. Phys. **83**, 1057–1110 (2011).
3 Alexei Kitaev, "Periodic table for topological insulators and superconductors," in AIP conference proceedings, Vol. 1134 (American Institute of Physics, 2009) pp. 22–30.

[4] Ching-Kai Chiu, Jeffrey C. Y. Teo, Andreas P. Schnyder, and Shinsei Ryu, "Classification of topological quantum matter with symmetries," Rev. Mod. Phys. **88**, 035005 (2016).

[5] Barry Bradlyn, L Elcoro, Jennifer Cano, MG Vergniory, Zhijun Wang, C Felser, MI Aroyo, and B Andrei Bernevig, "Topological quantum chemistry," Nature **547**, 298–305 (2017).

[6] Jorrit Kruthoff, Jan de Boer, Jasper van Wezel, Charles L. Kane, and Robert-Jan Slager, "Topological classification of crystalline insulators through band structure combinatorics," Phys. Rev. X **7**, 041069 (2017).

[7] Wladimir A Benalcazar, B Andrei Bernevig, and Taylor L Hughes, "Quantized electric multipole insulators," Science **357**, 61–66 (2017).

[8] Wladimir A. Benalcazar, B. A. Bernevig, and Taylor L. Hughes, "Electric multipole moments, topological multipole moment pumping, and chiral hinge states in crystalline insulators," Phys. Rev. B **96**, 245115 (2017).

[9] Frank Schindler, Ashley M Cook, Maia G Vergniory, Zhijun Wang, Stuart SP Parkin, B Andrei Bernevig, and Titus Neupert, "Higher-order topological insulators," Science advances **4**, eaat0346 (2018).

[10] Jongjun M. Lee, Chenhua Geng, Jae Whan Park, Masaki Oshikawa, Sung-Sik Lee, Han Woong Yeom, and Gil Young Cho, "Stable flatbands, topology, and superconductivity of magic honeycomb networks," Phys. Rev. Lett. **124**, 137002 (2020).

[11] Byungmin Kang, Ken Shiozaki, and Gil Young Cho, "Many-body order parameters for multipoles in solids," Phys. Rev. B **100**, 245134 (2019).

[12] William A. Wheeler, Lucas K. Wagner, and Taylor L. Hughes, "Many-body electric multipole operators in extended systems," Phys. Rev. B **100**, 245135 (2019).

[13] Raffaele Resta, "Quantum-mechanical position operator in extended systems," Phys. Rev. Lett. **80**, 1800–1803 (1998).

[14] F. D. M. Haldane, "Model for a quantum hall effect without landau levels: Condensed-matter realization of the "parity anomaly"," Phys. Rev. Lett. **61**, 2015–2018 (1988).

[15] Koji Kudo, Tsuneya Yoshida, and Yasuhiro Hatsugai, "Higher-order topological mott insulators," Phys. Rev. Lett. **123**, 196402 (2019).

[16] R. Nourafkan and G. Kotliar, "Electric polarization in correlated insulators," Phys. Rev. B **88**, 155121 (2013).

[17] Li He, Zachariah Addison, Eugene J Mele, and Bo Zhen, "Quadrupole topological photonic crystals," arXiv preprint arXiv:1911.03980 (2019).

[18] Arnob Kumar Ghosh, Ganesh C Paul, and Arijit Saha, "Engineering floquet higher order topological insulator by periodic driving," arXiv preprint arXiv:1911.09361 (2019).

[19] Qi-Bo Zeng, Yan-Bin Yang, and Yong Xu, "Higher-order topological insulators in two-dimensional aubry-andr\'e-harper models," arXiv preprint arXiv:1911.10816 (2019).

[20] Rui Chen, Chui-Zhen Chen, Jin-Hua Gao, Bin Zhou, and Dong-Hui Xu, "Higher-order topological insulators in quasicrystals," Phys. Rev. Lett. **124**, 036803 (2020).

[21] Qian Niu, D. J. Thouless, and Yong-Shi Wu, "Quantized hall conductance as a topological invariant," Phys. Rev. B **31**, 3372–3377 (1985).

[22] Joseph E. Avron and Ruedi Seiler, "Quantization of the hall conductance for general, multiparticle schrödinger hamiltonians," Phys. Rev. Lett. **54**, 259–262 (1985).

[23] Matthew B Hastings and Spyridon Michalakis, "Quantization of hall conductance for interacting electrons on a torus," Communications in Mathematical Physics **334**, 433–471 (2015).

[24] Koji Kudo, Haruki Watanabe, Toshikaze Kariyado, and Yasuhiro Hatsugai, "Many-body chern number without integration," Phys. Rev. Lett. **122**, 146601 (2019).

[25] Ken Shiozaki, Hassan Shapourian, Kiyonori Gomi, and Shinsei Ryu, "Many-body topological invariants for fermionic short-range entangled topological phases protected by antiunitary symmetries," Phys. Rev. B **98**, 035151 (2018).

[26] See the Supplemental Material for further details, which includes Ref. [7, 11–13, 21, 23–25, 36–38].

[27] Sinisa Coh and David Vanderbilt, "Electric polarization in a chern insulator," Phys. Rev. Lett. **102**, 107603 (2009).

[28] Here C_W counts the quantized pumping of the "physical" quadrupole moment, which is shown to be captured by the Wannier Chern number in Ref. [8].

[29] Yizhi You, FJ Burnell, and Taylor L Hughes, "Multipolar topological field theories: Bridging higher order topological insulators and fractons," arXiv preprint arXiv:1909.05868 (2019).

[30] Davide Ceresoli, T. Thonhauser, David Vanderbilt, and R. Resta, "Orbital magnetization in crystalline solids: Multi-band insulators, chern insulators, and metals," Phys. Rev. B **74**, 024408 (2006).

[31] Jörn W. F. Venderbos, Yichen Hu, and C. L. Kane, "Higher angular momentum band inversions in two dimensions," Phys. Rev. B **98**, 235160 (2018).

[32] Steven R. White, "Density matrix formulation for quantum renormalization groups," Phys. Rev. Lett. **69**, 2863–2866 (1992).

[33] Ulrich Schollwck, "The density-matrix renormalization group in the age of matrix product states," Annals of Physics **326**, 96 – 192 (2011), january 2011 Special Issue.

[34] Michael P Zaletel, Roger SK Mong, and Frank Pollmann, "Flux insertion, entanglement, and quantized responses," Journal of Statistical Mechanics: Theory and Experiment **2014**, P10007 (2014).

[35] Wonjun Lee, Gil Young Cho, and Byungmin Kang, *in preparation*.

[36] Seishiro Ono, Luka Trifunovic, and Haruki Watanabe, "Difficulties in operator-based formulation of the bulk quadrupole moment," Phys. Rev. B **100**, 245133 (2019).

[37] W. Kohn, "Analytic properties of bloch waves and wannier functions," Phys. Rev. **115**, 809–821 (1959).

[38] Christian Brouder, Gianluca Panati, Matteo Calandra, Christophe Mourougane, and Nicola Marzari, "Exponential localization of wannier functions in insulators," Phys. Rev. Lett. **98**, 046402 (2007).